BNL-212447-2019-JAAM

The Systematic Refinement for the Phase Change and Conversion Reactions Arising from the Lithiation of Magnetite Nanocrystals

C. N. Lininger, E. Takeuchi

To be published in "Advanced Functional Materials"

November 2019

Interdisciplinary Science Department

Brookhaven National Laboratory

U.S. Department of Energy

USDOE Office of Science (SC), Basic Energy Sciences (BES) (SC-22)

Notice: This manuscript has been authored by employees of Brookhaven Science Associates, LLC under Contract No. DE-SC0012704 with the U.S. Department of Energy. The publisher by accepting the manuscript for publication acknowledges that the United States Government retains a non-exclusive, paid-up, irrevocable, world-wide license to publish or reproduce the published form of this manuscript, or allow others to do so, for United States Government purposes.

DISCLAIMER

This report was prepared as an account of work sponsored by an agency of the United States Government. Neither the United States Government nor any agency thereof, nor any of their employees, nor any of their contractors, subcontractors, or their employees, makes any warranty, express or implied, or assumes any legal liability or responsibility for the accuracy, completeness, or any third party's use or the results of such use of any information, apparatus, product, or process disclosed, or represents that its use would not infringe privately owned rights. Reference herein to any specific commercial product, process, or service by trade name, trademark, manufacturer, or otherwise, does not necessarily constitute or imply its endorsement, recommendation, or favoring by the United States Government or any agency thereof or its contractors or subcontractors. The views and opinions of authors expressed herein do not necessarily state or reflect those of the United States Government or any agency thereof.

The Systematic Refinement for the Phase Change and Conversion Reactions Arising from the Lithiation of Magnetite Nanocrystals

Christianna N. Liningerξ, Andrea M. Bruckξ, Diana M. Lutz, Lisa M. Housel , Kenneth J. Takeuchi, Esther S. Takeuchi, Ashfia Huq, Amy C. Marschilok, Alan C. West**

*Author(s), and Corresponding Author(s)**

Dr. C. N. L. Author 1, Dr. A. M. B. Author 2, D. M. L. Author 3, L. M. H. Author 4, Prof. K. J. T. Author 5, Prof. E. S. T. Author 6, Dr. A. H. Author 7, Prof. A. C. M. Author 8, Prof. A. C. W. Author 9

E-mail: amy.marschilok@stonybrook.edu, acw7@columbia.edu

Dr. C. N. L. Author 1
Address where work was done: Department of Chemical Engineering, Columbia University, New York, NY, 10027, United States

Current Address: Chemical Sciences Division, Lawrence Berkeley National Laboratory, Berkeley, California, 94720, USA

Department of Chemical and Biomolecular Engineering, University of California, Berkeley, California, 94720, USA

Dr. A. M. B. Author 2

Address where work was done: Department of Chemistry, Stony Brook University, Stony Brook, NY, 11794, United States

D. M. L. Author 3

Department of Chemistry, Stony Brook University, Stony Brook, NY, 11794, United States

L. M. H. Author 4

Department of Chemistry, Stony Brook University, Stony Brook, NY, 11794, United States

Prof. K. J. T. Author 5

Department of Chemistry, Stony Brook University, Stony Brook, NY, 11794, United States

Department of Materials Science and Chemical Engineering, Stony Brook University, Stony Brook, NY, 11794, United States

Prof. E. S. T. Author 6

Department of Chemistry, Stony Brook University, Stony Brook, NY, 11794, United States

ξThese authors contributed equally to this work.

Department of Materials Science and Chemical Engineering, Stony Brook University, Stony Brook, NY, 11794, United States

Energy and Photon Sciences Directorate, Brookhaven National Laboratory, Upton, NY, 11973, United States

Dr. A. H. Author 7
Neutron Sciences Directorate, Oak Ridge National Laboratory, Oak Ridge, TN, 37831

Prof. A. C. M. Author 8
Department of Chemistry, Stony Brook University, Stony Brook, NY, 11794, United States

Department of Materials Science and Chemical Engineering, Stony Brook University, Stony Brook, NY, 11794, United States

Energy and Photon Sciences Directorate, Brookhaven National Laboratory, Upton, NY, 11973, United States

Prof. A. C. W. Author 9
Department of Chemical Engineering, Columbia University, New York, NY, 10027, United States

Department of Earth and Environmental Engineering, Columbia University, New York, NY, 10027, United States

Keywords: lithium-ion, batteries, phase identification, nanomaterials, thermodynamics

Nanostructured materials can exhibit phase change behavior that deviates from the macroscopic phase behavior. This is exemplified by the ambiguity for the equilibrium phases driving the first open circuit voltage (OCV) plateau for the lithiation of Fe_3O_4 nanocrystals. Adding complexity, the relaxed state for $Li_xFe_3O_4$ is observed to be a function of electrochemical discharge rate. The phases occurring on the first OCV plateau for the lithiation of Fe_3O_4 nanocrystals have been investigated with DFT through the evaluation of stable, or hypothesized metastable, reaction pathways. Hypotheses were evaluated through the systematic combined refinement with x-ray absorption spectroscopy (XAS), x-ray diffraction (XRD) measurements, neutron-diffraction measurements, and the measured OCV on samples

lithiated to x= 2.0, 3.0, and 4.0 in $Li_xFe_3O_4$. In contrast to the Li-Fe-O bulk phase thermodynamic pathway, Fe^0 is not observed as a product on the first OCV plateau for 10-45 nm nanocrystals. The phase most consistent with the systematic refinement is $LiFe_3O_4$, showing Li+Fe cation disorder. The observed equilibrium concentration for conversion to Fe^0 occurs at x =4.0. These definitive phase identifications relied heavily on the systematic combined refinement approach, which is broadly applicable to other nano- and meso-scaled systems that have suffered from difficult or crystallite-size dependent phase identification.

1. Introduction

1.1 Difficulty in Equilibrium Phase Identification for the Lithiation of Fe_3O_4

Using materials with intrinsically higher theoretical capacities for lithium-ion batteries will increase the lifetime and efficiency of current battery technologies. Magnetite, Fe_3O_4, is an inverse spinel material studied for potential use as an electrode material for Li-ion batteries with a theoretical capacity of 926 mAh/g utilizing its full conversion to Fe metal. However, the equilibrium phases driving the phase change reactions in magnetite, and the onset equilibrium concentrations for these phase changes, have remained elusive. Specifically, the first phase change in the material results in a "rocksalt-like" phase, precise identification of this phase remains unknown but is important in identifying irreversible phase changes known to occur in the Li-Fe-O system.[1] Investigations into the equilibrium phases driving the phase changes are needed, however, phase identification has proven to be difficult in this system due to topotactic phases occurring in the Li-Fe-O phase space and slow kinetics.[2] We therefore apply a systematic combined refinement in combination with density functional theory (DFT) studies to identify the equilibrium phases driving the phase change and conversion reactions occurring during the lithiation of magnetite. We identify the equilibrium phases for this system and also illustrate the usefulness of the combined refinement methodology that could be applied to other systems that suffer from difficult phase identification.

Adding to the difficulty of identifying phases in the Li-Fe-O ternary phase diagram, is that phases in this space have relatively small differences in heats of formation. The difference between the magnetite and maghemite[3] heat of formation is ~10 meV/atom, and Li_2O[4] and Li_5FeO_4[5] are ~40 meV/atom difference in formation energy. Due to the similarity in heats of

formation, a number of DFT calculated potentials are commensurate with experimentally measured voltages in the Li-Fe-O ternary space. Additionally, the overlap of reactions has been observed during lithiation of Fe_3O_4 nanocrystals under *in situ* lithiation observation, likely due to the similarity in heats of formation, slow kinetics of the chemical reactions occurring, and slow ion transport in the solid-state.[2] The phases resulting from these overlapping reactions have shown to be hard to distinguish spectroscopically due to high levels of structural similarity.

1.2 Systematic Combined-Refinement Approach for Phase Identification

Recently, guidelines for structural refinement of the lithium transition metal oxides were investigated where success of a combined-fit approach provided all structural parameters to be refined simultaneously which provides a model that more accurately reflects the structure than a single neutron or X-ray refinement alone. This approach leverages the enhanced sensitivity of neutron diffraction data on the oxygen coordinate and occupancy, Li occupancy and Li-metal mixing, and the enhanced d-range in the neutron experiments as well as the sensitivity to iron positions from the X-ray diffraction.[6] Due to the topotactic phases in the Li-Fe-O system, and their similarities in heats of formation, it is a model phase space to illustrate the utility of the combined refinement approach. We show that this methodology is necessary to definitively identify the phases occurring in the Li-Fe-O system.

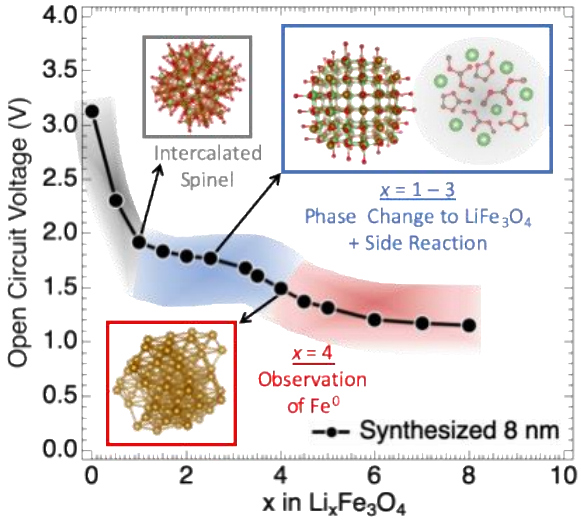

Figure 1: Experimentally measured open circuit potential for 8 nm Fe_3O_4 nanocrystals.[7] The initial intercalation regime is shown in grey, followed by the first phase change plateau in blue with the conversion plateau shown in red. The insets are graphical representations of the structural changes with lithiation where the box color corresponds to the color-shaded voltage regime.

1.3 Crystallite-Size Dependent Phase Change Behavior in Magnetite

Nanomaterials can exhibit crystallite-size dependent phase change behavior and it has been observed that the open circuit potential for lithiation of nanocrystalline magnetite varies with crystallite size.[8],[9] Upon full reduction of nanocrystalline (8-32 nm) Fe_3O_4 with lithium, there are three characteristic structural changes as indicated by the experimentally measured potential. The regimes are shown in **Figure 1** for 8 nm nanocrystalline Fe_3O_4,[7] with the intercalation regime shown in grey, the first phase change plateau in blue at ~1.8 V, and the conversion plateau in red at ~1.2 V. However, in micron-sized magnetite crystallites, only two regimes have been observed,[7-8, 10] an intercalation regime followed by a single voltage plateau at ~1.2 V.[8, 10] Yet, nanocrystals show two voltage plateaus at ~1.8 V and ~1.2 V as shown in **Figure 1**.

1.4 Regime 1: The Intercalation Regime in Nanoparticulate Magnetite

Magnetite is an iron oxide with an inverse spinel crystal structure, in the $Fd\overline{3}m$ space group and has been broadly studied for its magnetic, electronic, and application-based properties as far back as 1500 B.C.[11] Iron exists in two oxidation states in two different coordination environments, with the 8a tetrahedral A-site fully occupied by Fe^{3+} and the 16d octahedral B-site 50/50 by Fe^{2+}/Fe^{3+}. Oxygen defines the cubic close packed lattice at the 32e site.[12] Adding to the structural richness of this material, magnetite is known to be prone to off-stoichiometry, $(Fe_{8a})_1[Fe_{16d}]_{2-y}O_{4,32e}$, where y can range from 0 to 1/3.[13] At y=0.0, the stoichiometric magnetite is recovered, and at y=1/3 maghemite, γ-Fe_2O_3, forms with all iron at 3^+. The full open circuit potential for 8 nm Fe_3O_4 can be seen in **Figure 1**. The intercalation region in Fe_3O_4 for $0 < x <$ ~1.0, grey in **Figure 1**, has been recently attributed to lithium intercalation at iron defects at the 16d sites in nanocrystalline magnetite.

1.5 Regime 2: The Phase Change to a Rocksalt Phase

The intercalation regime is followed by the first voltage plateau at around ~1.8 V as illustrated in blue in **Figure 1**. This plateau represents the phase change where the inverse spinel structure is observed to transition to the rocksalt-like structure. The rocksalt-like phase is differentiated from the spinel phase by the observation of the tetrahedral iron migrating to the vacant 16c sites in the parent spinel. The detailed atomic identification of this rocksalt-like phase has been ambiguous and is the primary objective of this study as $LiFeO_2$, FeO, and $LiFe_3O_4$ can all satisfy the structural rocksalt observation and are related topotactically. This phase change is known to be due to the Coulombic interaction between iron at the 8a site in the

parent spinel and lithium inserting to the vacant 16c site. We recently showed that upon insertion of three Li^+ to three 16c sites surrounding an 8a iron, the 8a iron was fully displaced to an adjacent free 16c site:[14]

$$xLi + (Fe_1)_{8a}[Li_yFe_{2-y}]_{16d}O_{4,32e} \rightarrow \left(Fe_{1-\frac{x}{3}}\right)_{8a}[Li_xFe_{\frac{x}{3}}]_{16d}[Li_yFe_{2-y}]_{16d}O_{4,32e}$$

Reaction 1

The observation of a rocksalt-like phase on the first voltage plateau has been reported following lithiation to $Li_{1.5}Fe_3O_4$, where X-ray powder diffraction studies indicated the sample to be predominately rocksalt, with evidence of unreacted spinel.[10b] In another study, at *x*=1.7, a rocksalt phase was observed with 16% unreacted spinel remaining in the sample.[15] However, precise identification of the atomic structure of the "rocksalt-like phase" has remained elusive.[16] It is crucial that the rocksalt phase is identified due to the limited reversibility of the spinel-type Fe_3O_4 upon charge. EXAFS modeling has identified a reversible 'FeO-like' phase upon charge in EC and FEC based electrolytes to cycle 50 with no indication of tetrahedrally coordinated Fe which is indicative of the spinel structure.[17] It has also been previously identified that materials in the Li-Fe-O phase space are known to undergo irreversible phase change upon initial Li insertion, which inhibit full capacity retrieval upon cycling.[1] Additionally, the driving force for a crystalline phase may be low, illustrated by the small differences in heats of formation for phases in the Li-Fe-O ternary space. Further evidence for low driving force for a crystalline phase comes from our recent DFT study, where the rocksalt candidate $LiFe_3O_4$ was investigated. In the reported study, 97 symmetry unique ways to order Li+Fe on the 16c were tested. An ordering for Li + Fe on the 16c site in the $LiFe_3O_4$ phase was found to be 5 meV/atom more stable than phase segregation to the rocksalt-like $LiFeO_2$ + 2 FeO phases. However, more than one Li+Fe 16c cation ordering was found to be stable, with the energetics for the 97 different orderings essentially continuous. This indicated there was not one clear thermodynamically preferred cationic ordering for the $LiFe_3O_4$ phase.[14]

1.6 Regime 3: The Final Conversion Plateau

The Li-Fe-O ternary phase diagram in **Figure 2** indicates that BCC-Fe^0 is predicted to be a product in the $1 < x < 3$ concentration region, which corresponds to the first open circuit voltage plateau. Despite the thermodynamic prediction for iron metal formation on the first voltage plateau, room temperature studies have shown no evidence for iron formation for $0 < x < 2.0$ under relaxed conditions.[10a, 15] However, the Fe^0 + Li_2O conversion products have been

observed under discharge prior to the thermodynamically predicted concentration, and occurring in parallel with the first phase change reaction that results in the rocksalt structure.[2a, 15] The observation of Fe^0+ Li_2O prior to the thermodynamically predicted concentration further exemplifies the high mass transport limitations in the Li-Fe-O system.

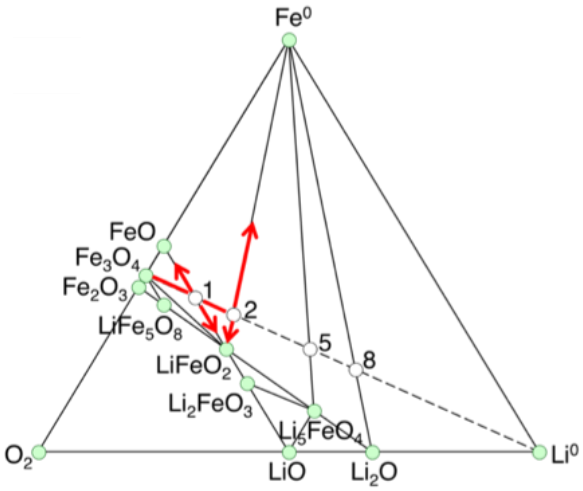

Figure 2: Li-Fe-O ternary phase diagrams with known stable phases in green, the lithiation of magnetite as a dashed line, and white open circles indicating *x* for $Li_xFe_3O_4$ lithiation states. The red lines indicate the pathway that is thermodynamically predicted to occur on the first voltage plateau.

1.7 Previous Theoretical Studies of The Two Voltage Plateaus of the Reversible Potential

DFT calculations have been used to predict the reversible potential for two competing pathways for the full $0 < x < 8$ equivalents.[2a] One of the pathways was guided by the stable phases on the Li-Fe-O ternary diagram and is the thermodynamically predicted equilibrium path. The second proposed pathway was metastable and motivated by the experimentally observed phases occurring *in situ*. In both pathways, lithiation results in the formation of the rock-salt $LiFe_3O_4$ phase. In the equilibrium pathway, further lithiation of $LiFe_3O_4$ resulted in $LiFeO_2$+Fe^0, followed by three additional steps continuing to form BCC-Fe^0. This equilibrium pathway predicted that Fe^0 is formed on the first voltage plateau. The second pathway was a two-step process where the $LiFe_3O_4$ phase converted directly to the Li_2O+Fe^0 conversion products.[14] The study was primarily focused on the reaction kinetics far from equilibrium and discharged at high rates, under conditions relevant to device operation, where both proposed pathways could be occurring in parallel.

1.8 The Need for An Integrated Approach to Phase Identification for the First Voltage Plateau

In this work, in order to identify the equilibrium phases driving the phase change corresponding to the first voltage plateau, a series of hypotheses were developed that satisfied several constraints. Due to the experimental observation that through full lithiation the ccp oxygen network remains invariant, the first constraint was to only study phases within the Li-Fe-O space that had a ccp rocksalt-like structure.[18] Secondly, the hypotheses satisfied the constraint of the nominal lithium concentrations allowed on the first voltage plateau, ~1-2 equivalents. Third, the hypotheses satisfied the voltage observed experimentally, ~1.8 V. Experiments were performed at very low rates, as close to equilibrium conditions as possible, with slow lithiation and relaxation time included in the preparation of the lithiated samples. The lithiated samples were characterized using complementary techniques of x-ray absorption spectroscopy (XAS), x-ray diffraction (XRD) measurements, and neutron-diffraction measurements to identify for the first time the equilibrium phase forming on the first open circuit voltage plateau. There is more than one phase in the Li-Fe-O space that satisfies the requirement of a rocksalt-like phase, differing in the orderings of octahedrally coordinated Li and Fe (the topotactically related phases). More than one combination of these phases also predicts a voltage with DFT that is comparable to the experimental voltage of 1.8 V for this first plateau, consistent with the similarities in heats of formation in the Li-Fe-O ternary space, adding to the difficulty of precise identification. This study on the Li-Fe-O space illustrates the importance of the combined refinement approach for the examination of electrochemical conversion/phase change processes in systems with elusive or ambiguous phases.

2. Methods

2.1. Electrochemical Measurements

The 30 nm Fe_3O_4 was synthesized using a co-precipitation method previously reported.[19] The positive electrode was caste on copper foil using carbon (20%), polyvinylidene fluoride binder(10%), and nanocrystalline Fe_3O_4 (70%) active material. Coin type cells used lithium anodes, 1 M $LiPF_6$ in 7:3 by volume ratio of dimethyl carbonate (DMC) and ethylene carbonate (EC) electrolyte, and were assembled under argon atmosphere. Samples for neutron and x-ray diffraction were prepared using 90% Fe_3O_4, 7% carbon, and 3% polytetrafluoroethylene binder. The Fe_3O_4 was lithiated at 37 mA/g Fe_3O_4 to 1, 2, 2.5, 3, or 4 molar equivalents. Cells were relaxed for at least 37 hours after being discharged prior to material recovery.

2.2. XRD, XAS, and Neutron Diffraction Measurements

Electrodes were handled under inert atmosphere and sealed in polyimide tape for XAS analysis. XAS spectra were collected at Argonne National Laboratories Advanced Photon Source beamline 12-BM. All measurements were collected at the Fe K-edge (7112 eV) with a metal foil reference collected simultaneously with each lithiation condition. Each spectrum was aligned and normalized in Athena.[20] The EXAFS fitting was performed in Artemis with structural models generated from FEFF6.[21] The structural models were the spinel Fe_3O_4, the rocksalt FeO phase, and body-centered cubic Fe metal with each fit in the k-range 3-10 Å (dk = 2) in k, k^2, and k^3 weights and R-range was from 1-4 Å.

The samples for neutron diffraction were packed into vanadium tubes for measurement. The neutron diffraction was Time-of-flight (TOF) powder neutron diffraction conducted at POWGEN (BL-11A) diffractometer at the Spallation Neutron Source (SNS), Oak Ridge National Laboratory, Oak Ridge, Tennessee. Polyimide tubes were used to hold the samples for XRD diffraction data collection. Monochromatic x-ray powder diffraction (XRD) was performed *ex situ* (λ=0.1885 Å) at Brookhaven National Laboratories (BNL) National Synchrotron Light Source II (NSLS-II) beamline 28-ID. The beam was calibrated to a wavelength of 0.1885 Å and used a 16-inch CsI scintillator detector for the collection of 2D images that were integrated to 1D diffraction data using a LaB_6 standard. Rietveld refinement was performed using GSAS-II software where the neutron and X-ray diffraction date were fit to a single structural model.[22]

In situ XRD during the first cycle was conducted as previously described.[2b] Specially designed *in-situ* cells used Li metal, polyethylene separator, 1 M $LiPF_6$ in 3:7 EC:DMC (v/v) electrolyte, and Fe_3O_4 electrodes. XRD scans were collected with a 0.1° step size at a scan rate of 2°/min by a Rigaku Mini-Flex X-ray powder diffractometer during to x = 3 in $Li_xFe_3O_4$ at C/25 controlled by a Bio-Logic Science Instruments potentiostat.

2.3. First Principle Calculations Methods

A zero temperature Li-Fe-O ternary phase diagram was constructed in a previous DFT study of the energetics of lithiation of magnetite.[14] All calculations were performed with Vienna ab initio simulation package (VASP)[23] with projector augmented wave potentials,[23-24] with an energy cutoff of 600 eV. To account for the Coulomb interactions in the 3d orbitals of Fe, U_{eff}=5.3 eV was used.[25] In the case of Fe^0, an effective U was not applied, as it is not physically reflective of the conductive electronic structure. To ensure accurate prediction of reaction energies which include both Fe^0 and materials with correlation in 3d orbitals,

corrections were applied to account for mixing of GGA and GGA+U from the methodology developed by Jain et al.[25c] The corrections impacted the reaction energies, and therefore the voltages, when Fe^0 is a reactant or product. The generalized gradient approximation by Perdew, Burke, and Ernzehof (PBE) was used for the exchange-correlation energy.[26] A Γ-centered grid defined by a 3×3×3 mesh for the cubic Fe_3O_4 structure was used for Brillouin zone sampling. The mesh was scaled appropriately for structures sampled in different supercells, and is previously reported.[14] The Methfessel-Paxton smearing scheme of order 1 with a broadening parameter of 0.2 eV was employed. Total energies were found to converge to within 2 meV/f.u and a minimum force criterion of 0.05 eV/Å was applied. Cells were allowed to relax fully without imposing symmetry.

2.4 Prediction of Potential

Equilibrium voltages have been predicted from the DFT calculations in the Li-Fe-O ternary phase space. To arrive at voltages from DFT calculated energies, a stoichiometrically consistent reaction is written out, and the energy change upon reaction, A + nLi^0 → C, is computed with energies from the DFT calculations. The result is the zero-temperature energy change for reaction, $\Delta E_f = E(C) - E(A) - nE(Li^0)$. The voltage is then determined from the reaction energy, $V = -\frac{\Delta E_f}{nF}$, where *n* is the number of electrons passed in the reaction. We direct readers to the review papers on the methodology relating the DFT calculated zero temperature energy difference to equilibrium potential for more information.[27]

In the case of a phase change reaction, the voltage is constant for all concentrations on the plateau. Herein, we plot the phase change voltage over the full concentration range sampled. For instance, for a reaction where 1 electron is transferred, we plot the DFT predicted potential over a range of Δx =1.0. Where indicated, the potential is not necessarily plotted starting at the nominal *x* value indicated by the reaction, but is always plotted for the calculated Δx. For instance, the reaction Fe_3O_4 + Li → $LiFe_3O_4$ may be plotted starting at a nominal x value on the x-axis of *x*=1.0 and lasting until *x*=2.0. In the case where there is a discrepancy between the *x* indicated by the reaction and the *x* that the DFT calculated potential is plotted at can be attributed to side reaction and defect filling occurring between nominal *x*=0.0 and *x*=1.0 as and will be further discussed.

3. Results

3.1. Measured and DFT Predicted Reversible Potential

There are differences in the 10 nm versus the 30 nm crystallite size Fe_3O_4 open circuit potential versus lithium at low depths of discharge (x<1.0), previously understood by variations in the concentration of Fe cationic defects as a function of crystallite size.[28] However, on the first voltage plateau, the 10 nm and 30 nm Fe_3O_4 nanocrystallites exhibit the same open circuit potential versus lithium, ~1.8 V, illustrated in **Figure S.1**.

As indicated in **Figure 1**, the open circuit potential is split into three known structural changes and one unexplored regime. Due to differences in sample stoichiometry, the maximum concentration for each of these regimes can be a function of nanocrystallite size. In order to clearly define each regime, a voltage cutoff has been defined, where the voltage cutoff for the intercalation regime is 1.88 V and the voltage cutoff for the first phase change plateau is 1.68 V. The intercalation regime is defined as being completed at the concentration at which the potential crosses 1.88 V. Similarly, the first voltage plateau is defined as being completed at the concentration at which the potential reaches 1.68 V. The length of the first phase change plateau is therefore Δx~2 as seen in **Figure 1** (blue). Following the first phase change plateau, the conversion plateau is observed at ~1.2 V, lasting for Δx~3 in **Figure 1** (red).

3.2. Hypothesized Reactions Occurring on First Phase Change Plateau

In total, fifteen hypothesized reaction mechanisms were tested, where nine yielded DFT calculated equilibrium potentials that satisfy the experimental potential of 1.8 V, which are shown in **Table 1**. According to the ternary phase diagram in **Figure 2,** Fe metal is predicted to form on the first phase plateau. To assess the formation of this phase, in four of the pathways, (a-d), BCC-Fe^0 is predicted to form, while the other five do not involve the formation of iron (e-i). The experimentally observed plateau potential is ~1.8 V, the five DFT predicted potentials that are within 100 mV of the experimental value are shown in bold, (a,d,g,h, and i), these hypotheses are closest to the experimentally measured potential and are considered in good agreement. The remaining three hypotheses between $\pm$100-200 mV of the experimental potential are shown in regular type, (b, c, and f) and are considered in moderate agreement with experiment. The lowest energy hypothesis, (e), is shown in italics as it is 300 meV above the measured potential. This lowest energy phase in hypothesis (e), $LiFe_3O_4$, was recently discovered in a theoretical examination of the x =0 to 1 region and is a new addition to the Li-Fe-O phase diagram.[14]

As seen in the open circuit potential in **Figure 1**, the first phase change plateau starts at *x~1.*0 and lasts for Δx~2.0 equivalents of lithium, to x~3.0. At low depths of discharge (*x~0.5)*

and on the first voltage plateau *(x~1-3)* side reactions with electrolyte have been observed to occur during electrochemical discharge of the Fe_3O_4 active material.[29] Therefore, the concentration of lithium in the starting material in **Table 1** is indicated as 'y', and the value can be less than or equal to the discharged value of *x*~1.0, but is not precisely known due to side reaction. Additionally, the starting concentration of iron in the sample can vary due to cationic defects.[30] For each hypothesis in **Table 1**, the Δx for the phase change is indicated in the second column, under the DFT predicted voltage. As can be seen, not all hypotheses account for the full Δx=2.0 equivalents electrochemically passed on the first voltage plateau, but are included as the products are in the correct concentration range on the ternary phase diagram and they are predicted to occur in combination with a parallel, non-Faradaic reaction.[2a],[29-30]

Table 1: Hypothesized reactions for the first voltage plateau and the conversion plateau with the corresponding DFT predicted voltages, and equivalents of lithium allowed for each reaction.

Hypotheses for Reaction Pathway on First Voltage Plateau	DFT Predicted Voltage and **Δ**x for Phase Change
Iron Extrusion	
a) $Li_yFe_3O_4$+ ΔxLi^0 → 2 $LiFeO_2$ + Fe^0	**1.9 V Δx=2-y**
b) $Li_yFe_3O_4$+ **Δ**xLi^0 → 0.57 Li_2O + 0.86 $LiFe_3O_4$ + 0.43 Fe^0	1.6 V Δx=2-y
c) $Li_yFe_3O_4$+ **Δ**xLi^0 → Li_2O + 0.75 Fe^0 + 0.75 Fe_3O_4	1.6 V Δx=2-y
d) $Li_yFe_3O_4$+ ΔxLi^0 → 0.4 Li_5FeO_4 + 0.8 Fe^0 + 0.6 Fe_3O_4	**1.7 V Δx=2-y**
No Iron Extrusion	
e) $Li_yFe_3O_4$+ **Δ**xLi^0 → *$LiFe_3O_4$*	*2.1 V* Δx=1-y
f) $Li_yFe_3O_4$+ **Δ**xLi^0 → 2 FeO + $LiFeO_2$	2.0 V Δx=1-y
g) $Li_yFe_3O_4$+ ΔxLi^0 → 0.5 $LiFeO_2$ + 2.5 FeO + 0.5 Li_2O	**1.7 V Δx=1.5-y**
h) $Li_yFe_3O_4$+ ΔxLi^0 → 0.5 $LiFe_3O_4$ + 1.5 FeO + 0.5 Li_2O	**1.8 V Δx=1.5-y**
i) $Li_yFe_3O_4$+ ΔxLi^0 → 3 FeO + Li_2O	**1.8 V Δx=2-y**

3.3. X-ray Absorption Spectroscopy to identify Fe metal formation

According to the Li-Fe-O ternary phase diagram as well as phases observed during discharge, one of the major competing reactions at x = 2 for the lithiation of Fe_3O_4 is the formation of Fe metal. XAS was used to identify the formation of nanosized Fe metal as a result of the lithiation process. Based on stoichiometry, if iron formed at x=2.0 it could be identified by spectroscopic techniques.[31] Fe metal nanoparticles were used for reference in the near-edge (XANES) region of the spectra to identify the shifting during electrochemical reduction

and in the extended fine structure (EXAFS) a full fit using contributions from FEFF6 calculations was used to identify Fe-Fe metal contributions.

The lithiation and voltage recovery curves of the Li/Fe_3O_4 cells are shown in **Figure S2** where the x =1 (in $Li_xFe_3O_4$) sample remains above 1 V and the other conditions (x = 2-4) reach a loaded voltage between 0.84 - 0.9 V before recovery. Additionally, side reactions have been documented at these low potentials in Li/Fe_3O_4 cells.[30] The XANES region for each sample is shown in **Figure 3a** where the Fe K edge positions are shown to shift to lower energy with continued lithiation, consistent with the reduction of $Fe^{2/3+}$. Notably, the edge shift from x = 0 to 1 is from 7126.1 to 7124.1 eV, respectively, showing a significant change in the oxidation state of the Fe metal center. However, from x = 2 to 4 there is less than a 0.1 eV shift in the edge energy, consistent with previously observed side reactions occurring at these potentials.[17, 30] The largest change in the overall oxidation state occurs in the initial insertion of lithium into the spinel structure.

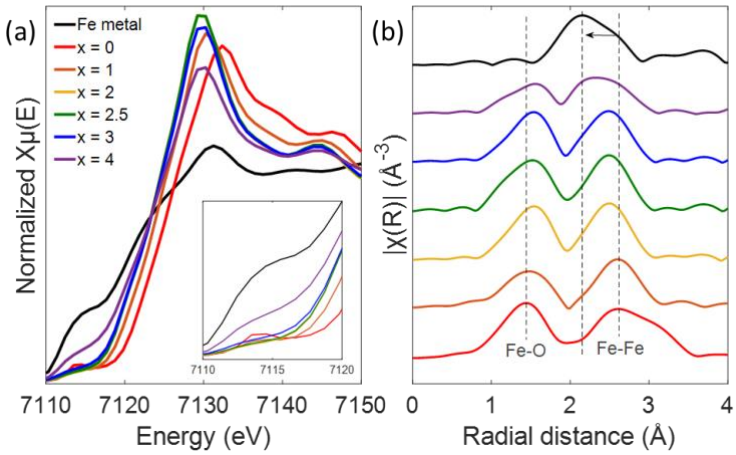

Figure 3: (A) XANES region of the lithiated Fe_3O_4 material series with Fe metal nanoparticles shown as a reference material. The inset shows the pre-edge region. (B) The EXAFS region of the lithiated Fe_3O_4 material series where the Fe-O and Fe-Fe contributions are identified and compared to Fe metal nanoparticles.

A notable feature in the Fe K edge is the pre-edge region which has been shown to change based on oxidation state and coordination environment.[32] Based on this region, from x = 1 to 2, the coordination of the one third of the Fe centers change from tetrahedrally coordinated Fe to all octahedrally coordinated. In the x = 0 sample (**Figure 3a**) a pre-edge peak is observed below 7115 eV and upon electrochemical reduction the pre-edge peak diminishes by x = 2, providing further evidence of the change in coordination to all octahedral sites. From

x = 1 to 3 only minor shifting in the pre-edge is observed which provides evidence of hindered redox activity in that range of the lithiation process. Once *x* = 4 is reached, the pre-edge shows significant shifting closer to the Fe metal pre-edge consistent with the onset of Fe metal formation as has been previously observed upon *in situ* lithiation of Fe_3O_4.[30]

To better understand the transition from spinel to rocksalt and the final conversion to Fe metal, EXAFS spectra were modeled using Artemis to identify the local atomic structure of Fe in the early lithiation process where the fitting results are shown in **Figure S3** and **Table S1, S2, and S3**. For the unlithiated and *x* = 1 materials the model used the inverse spinel structure with tetrahedral Fe-O and Fe-Fe contributions and the octahedral Fe-O and Fe-Fe contributions. From the *x* = 0 to 1 structure the octahedral Fe-O interatomic distances expand from 1.96 +/- 0.01 to 2.04 +/- 0.02 Å and 3.56 +/- 0.01 to 3.65 +/- 0.02 Å indicating the lattice expansion associated with Li insertion into the octahedral vacancies. Upon lithiation to *x* = 2 the tetrahedral contribution was no longer needed for the modeling and a FeO-type all octahedral model was used. From *x* = 2 to 4 there was little deviation in the interatomic distances of the octahedral Fe. The nearest neighbor values decrease at *x* = 4 consistent with decrease of the crystallite size and necessitates the addition of the Fe-Fe contributions of Fe metal. Fe metal contribution can clearly be seen in **Figure 3b** and has been fully modeled in **Figure S3f**. The incorporation of Fe metal was not necessary until *x* = 4 and therefore, the Fe formation reaction pathways for the rocksalt structure of lithiated $Li_xFe_3O_4$ at *x* = 2 were eliminated for the electrochemical conditions used in this investigation.

3.4. Combined Refinement of X-ray and Neutron Diffraction to Identify the Rocksalt Structure at *x*=2.0

To determine the structure of the phase forming at *x*=2.0, a combined Rietveld refinement using neutron and x-ray powder diffraction of the rocksalt phase was performed. The combined refinement leverages the enhanced sensitivity of neutron diffraction data on the oxygen coordinate and occupancy, Li occupancy and Li-metal mixing, and the enhanced d-range in the neutron experiments as well as the sensitivity to iron positions from the X-ray diffraction. Recently, guidelines for structural refinement of the lithium transition metal oxides were investigated where success of the combined fit provided all structural parameters to be refined simultaneously which provides a model that more accurately reflects the structure than a single neutron or X-ray refinement alone.[6]

Due to the lack of evidence for Fe nanoparticles at *x*=2.0 from the XAS analysis in the previous section, the competing reactions which included Fe metal formation were not considered, pathways (e)-(i) in **Table 1**. A number of Li/Fe-containing structures were calculated with DFT including $LiFe_3O_4$, FeO, and $LiFeO_2$ with mixtures of those phases to varying degrees and the possible incorporation of Li_2O, all outlined in **Table 1**. The DFT predicted structures are shown in **Figure 4a-c**, where the Fe-O arrangement is identified. For the FeO phase there is alternating stacking between Fe and O. The $LiFe_3O_4$ phase contains a disordered Li-Fe-O arrangement where the Li occupancy prefers the '16c' site compared to the '16d'[8], and finally the $LiFeO_2$ phase contains ordered layers of Fe-O-Li in the calculated unit cell. The structures for the refinement were the DFT calculated structures for FeO and $LiFeO_2$ as illustrated in **Figure 4a/d** and **c/f.** The $[LiFe]_{16c}[Fe_2]_{16d}O_4$ (LiFe3O4) phase was recently shown to have a low driving force for the formation of a highly crystalline equilibrium phase[14] therefore, the $LiFe_3O_4$ structure for refinement had mixed occupancy of Li+Fe on 16c site, as shown in **Figure 4e.**

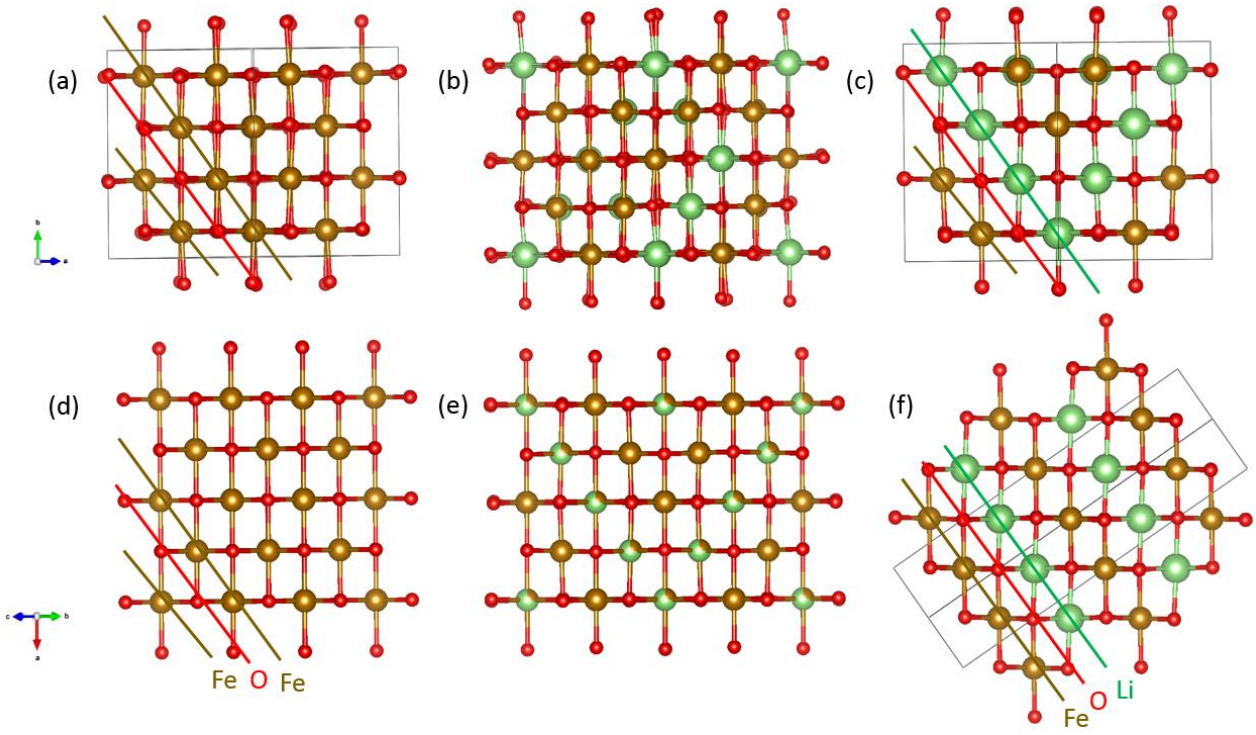

Figure 4: DFT simulated structures of (a) FeO, (b) $LiFe_3O_4$, and (c) $LiFeO_2$ and the symmetric structures used for refinement with (d) FeO with Fm-3m space group, (e) $LiFe_3O_4$ with Fm-3m space group, and (f) $LiFeO_2$ with an R-3m space group.

The FeO model used an Fm-3m space group which defines only one distinct Fe position and provides Fe-O-Fe stacking. To maintain consistency with the parent spinel, the $LiFe_3O_4$ used

the Fd$\overline{3}$m which defines two separate Fe positions, and Fe-Li mixing in the 16c position is allowed. The final $LiFeO_2$ structure uses R$\overline{3}$m symmetry which allows for the Fe-O-Li stacking. Note that all of these structures contain a $\overline{3}$m symmetry element and contain Li and Fe in octahedral coordination only, as they occur in their lowest energy phases on the Li-Fe-O diagram. Also, the oxidation states of Fe in these phases vary, where FeO contains only Fe^{2+}, $LiFe_3O_4$ contains $Fe^{2.33+}$, and $LiFeO_2$ contains Fe^{3+}. Based on the Coulombically controlled Li insertion, if all of the Li^+ ions are associated with the Fe redox then the oxidation should be Fe^{2+}. However, as noted by previous investigations of side reactions occurring during the first discharge, it is possible to decompose electrolyte and form an SEI at potentials lower than 1 V hindering the reduction of Fe,[17, 30] and as observed in **Figure 1**, the loaded voltage goes below 1 V for all x>1.5.

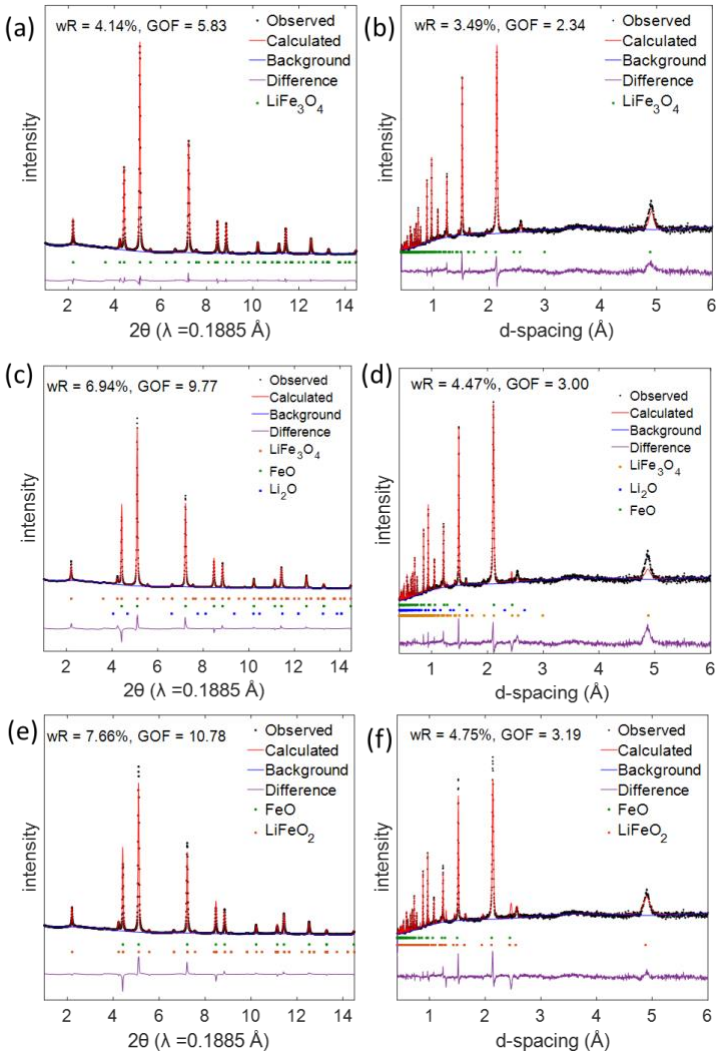

Figure 5: Rietveld refinement of combined TOF neutron diffraction and X-ray diffraction data to a single set of structural parameters for rocksalt structure with the (a) XRD and (b) TOF data for to the '$LiFe_3O_4$' condition, (c) XRD and (d) TOF data for to the '$LiFe_3O_4$+ FeO + Li_2O' condition, and (e) XRD and (f) TOF data for to the '$LiFeO_2$ + FeO' condition.

In **Figure 5a-b**, the combined refinement of the $LiFe_3O_4$ phase is shown, where all of the observed reflections are accounted for by the single phase, the additional refinement parameters can be found in **Table 2**. The lattice parameter a = 8.46197(4) Å with the crystallite size = 44.2 +/- 0.3 nm and the microstrain of 0.227 +/- 0.006%. Also, considerable mixing of the Fe-Li at the 16c and 16d sites was observed, where the 16d site contains 0.946(7) occupancy Fe and the 16c has 0.537(4) supporting the XAS observation of tetrahedral Fe migration to the octahedral site upon lithiation to *x*=2.0 in the previous section. The remaining occupancy at those positions is saturated with Li providing the final stoichiometry of $Li_{1.03}Fe_{2.97}O_4$. Although there is excellent agreement with the diffraction modeling, the combined refinement was applied to DFT identified Reaction Pathway (h) in **Table 1**, FeO + $LiFe_3O_4$ + Li_2O (**Figure 5c-d**), and DFT identified Reaction Pathway (g) in **Table 1**, FeO + $LiFeO_2$ (**Figure 5e-f**), based on the discrepancy between the electrochemically discharged lithium concentration and Fe redox state.

Table 2: Structural parameters for rocksalt structure with the '$LiFe_3O_4$' condition obtained from combined Rietveld refinement of TOF neutron diffraction and X-ray diffraction data.

Space group: Fd-3m a = 8.46197(4) Å Crystallite size = 44.2 +/- 0.3 nm, Microstrain = 0.227 ± 0.006%, Volume = 605.920(9) Å^3					
Atom	**x**	**y**	**z**	**Occupancy**	**Uiso**
Fe	0.5	0.5	0.5	0.946(7)	0.0134(5)
Fe	0.0	0.0	0.0	0.537(4)	0.00513(8)
Li	0.5	0.5	0.5	0.054(7)	0.03(1)
Li	0	0	0	0.463(4)	0.03(1)
O	0.2526(1)	0.2526(1)	0.2526(1)	1.0	0.008
X-ray: wR = 4.14%, GOF = 5.83 Neutron: wR = 3.49%, GOF = 2.34					

3.5. Combined Refinement of X-ray and Neutron Diffraction on Additional Rocksalt Phases

Refinement of the neutron and X-ray diffraction data for all of the possible phases on the first voltage plateau show the subtle variation in structure and patterns. In **Figure 5a-b**, the combined refinement of the $LiFe_3O_4$ phase is shown, this was the best statistical fit with the X-

ray data (**Figure 5a**) providing an wR = 3.49% and the best statistical fit with the TOF neutron diffraction (**Figure 5b**) at wR = 4.14%. Additionally, the $LiFe_3O_4$ fit determined lattice parameter was a = 8.46197(4) Å with the crystallite size = 44.2 +/- 0.3 nm and the microstrain of 0.227 +/- 0.006%, a change of 0.06127 Å from the pristine Fe_3O_4 nanocrystal measured at a=8.4007 Å. This is in excellent agreement with the DFT predicted lattice constant change of 0.06836 Å from the DFT calculated phase of Fe_3O_4 to the DFT calculated $LiFe_3O_4$ phase.[14]

The obvious phase for the reduction of Fe_3O_4 would be FeO. In DFT identified Reaction Pathway (i), FeO forms with Li_2O as the lithium sink. However, the introduction of FeO results in a mismatch of relative peak intensities from the FeO phase where the FeO(111) contributes a higher intensity than observed and the FeO(200) and (220) do not provide adequate intensity for the observed pattern (**Figure S4**). The FeO(111) is an all Fe containing lattice plane, therefore the introduction of the Li in the 16c sites likely contributes to the dampened scattering observed experimentally. Reaction pathway (h) suggested by DFT in **Table 1** results in the products 0.5 $LiFe_3O_4$ + 1.5 FeO + 0.75 Li_2O where $LiFe_3O_4$ and FeO in a 1: 3 molar ratio, respectively. The combined refinement of this pathway is shown in **Figure 5c-d** resulting in a FeO of 49.3 +/- 0.4 wt% which matches the predicted value. However, even with the addition of $LiFe_3O_4$, this refinement still shows the mismatch of intensities due to the high concentration of the FeO phase and the missing reflections in the neutron pattern.

To address all phases identified by DFT in **Table 1**, the final phase combination of $LiFeO_2$ + 2 FeO from Reaction Pathway (f) was also calculated with the fit and fit parameters shown in **Figure 5 e-f** and **Table S5**. Here the reported weight fractions are 76 +/- 5 wt% for FeO and 24 +/- 4 wt% for $LiFeO_2$ which also agrees with the predicted DFT ratio. However, the fit is plagued by the same intensity issues already discussed with the FeO phase, but the reflection at d = 4.88 Å is accounted for by the $LiFeO_2$(003) reflection. Although there is a reasonable match with the larger d-spacing reflections when looking at the neutron diffraction data between 1.5 - 0.4 Å (**Figure S5**), it is indicated by the $LiFeO_2$(331), (333), and (553) at d = 0.9708, 0.8144, and 0.5509 Å, respectively (**Figure 5e**), that this is not the best match to the observed pattern.

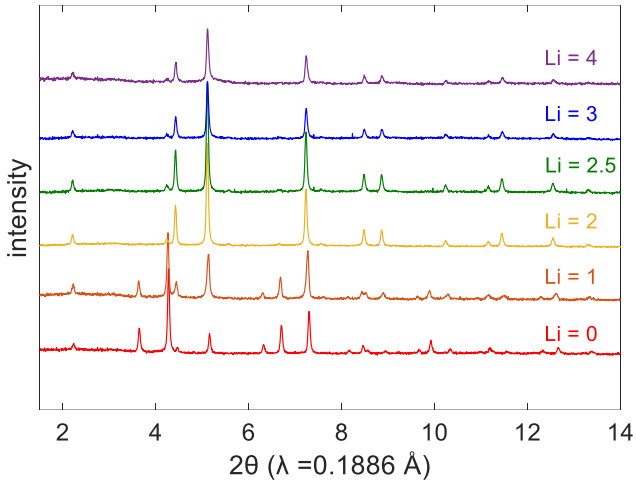

Figure 6: *Ex situ* XRD patterns of $Li_xFe_3O_4$ at different lithiation levels.

3.6. X-ray Diffraction to Identify $LiFe_3O_4$ Onset and Persistence

Additional *ex situ* XRD experiments were used to (1) identify the lithiation level where the rocksalt formed during electrochemical discharge, and (2) screen the persistence of the $LiFe_3O_4$ phase up to x = 4 and are shown in **Figure 6**. Upon lithiation the spinel transformation to the rocksalt phase can be seen by the change in peak intensity from x = 0 to 2. At this point, the Fe_3O_4(311) is the most intense peak which gradually shifts to the $LiFe_3O_4$(200) at x=2. As noted before, the $LiFe_3O_4$(111) reflection at d = 4.89 Å is observed at x =2 up to x = 4 and there is also no considerable change in relative peak intensity or peak shifting despite continued electrochemical discharge. These reflections and their presence throughout discharge have been reported in multiple lithiation investigations of Fe_3O_4.[2a, 15] The retention of these peaks indicate that the $LiFe_3O_4$ phase is likely still the predominant phase at x =4 and directly converts to Fe metal and Li_2O which has previously been suggested.[2a]

4. Discussion

4.1 DFT Predicted Potentials for First Voltage Plateau

As is seen in **Table 1**, DFT predicts multiple reactions give a reasonable range for the DFT prediction of voltage, while also satisfying the number of electrons passed on this first voltage plateau. These reaction pathways offer a starting point for possible phases forming in the experimental system. However, in realistic phase spaces such as Li-Fe-O, with similar heats or formation and homologous crystal structures, these theoretical results also illustrate that the prediction of the open circuit voltage with DFT can be insufficient to isolate any one reaction pathway, emphasizing the utility of iterative theory and systematic refinement practices.

4.2 Absence of Evidence for Fe^0 in XAS Measurements

The assessment of the thermodynamically predicted Fe^0 phase at x=2.0 (**Figure 2**) was interrogated with XAS analysis. The XAS spectra were collected and analyzed for the variation in oxidation state via the XANES region and the presence of Fe-Fe metal contributions in the EXAFS region. The XANES analysis showed the highest change in edge energy from x = 0 to 1 with minimal additional shifting up to x = 4. However, the EXAFS region showed a significant shift from x = 3 to 4. Therefore, the largest change in the Fe redox happened between x = 0 to 1 with additional change in Fe redox state occurring from x = 3 to 4, while the region between x = 1 to 3 was observed to have hindered Fe redox activity.

To investigate this further, the full fitting of the EXAFS region was performed where the spinel structure with tetrahedral Fe were used for x = 0 to 1. All fits for x> 1.0 only included the octahedral coordination, as tetrahedral coordination was inconsistent. Finally, at x = 4 the incorporation of Fe-Fe metal contributions was necessary to obtain a high-quality fit. Based in the results of this work, previous TEM studies and other EXAFS investigations of the lithiation of $Li_xFe_3O_4$, at x=2.0, Fe^0 is not evidenced to be forming in any spectroscopically distinguishable form[2, 15, 18] and the phase change to the $LiFe_3O_4$ rocksalt structure occurring between x = 1 to 3 occurs in parallel with side reactions that consume the discharged lithium, as the Fe redox activity is hindered here.

4.3 Neutron and X-ray Diffraction Measurements and Combined Refinement for $Li_xFe_3O_4$ at x=2.0

The pathway competing with the formation of $LiFe_3O_4$ on the Li-Fe-O phase diagram in **Figure 2** is the formation of $LiFeO_2$ + 2 FeO. An important observation from the combined neutron and X-ray fits was the $LiFe_3O_4$(111) reflection at d = 4.89 Å in **Figure 5a**. This reflection was difficult to model with a mixture of phases containing the FeO material because FeO did not have any reflections in this region. These variations in intensity and reflections are even more apparent when removing the $LiFe_3O_4$ phase altogether and only fitting the FeO phase, as shown **Figure S4**. Here the relative intensities of the peaks are very different from the observed pattern which is demonstrated by the increase in wR and goodness of fit parameters (fit parameters reported in **Table S6**). Particularly in the X-ray diffraction, the FeO does not account for all the observed reflections and the relative intensities in the observed pattern. This shows that a Fe-O only rocksalt structure with no Li-Fe mixing does not account for all of the observed

reflections, and that the $LiFe_3O_4$ phase without FeO most accurately describes the observed diffraction patterns.

The systematic refinement based on the DFT identified competing Reaction Pathways in **Table 1** indicates that the $LiFe_3O_4$ phase is the most consistent structural model with the experimental data. This structure shows a disordered Fe-Li mixing at two distinct Fe sites that are retained from the parent spinel phase upon electrochemical reduction. The reflections of all of these phases were very similar, but the variations between the X-ray and neutron combined refinement allowed a high-quality fit using the higher d-spacing range from the neutron diffraction. To the authors' knowledge, there has not been another systematic study that has attempted to differentiate the thermodynamic pathway from the kinetic phases observed during discharge, and eliminating the other possible reaction pathways via XAS, X-ray, and neutron diffraction. The result is that we have definitively identify the equilibrium phase forming on the first voltage plateau as $LiFe_3O_4$. This allows us to say with a high degree of certainty that the thermodynamically stable rocksalt phase formed on the first voltage plateau is the reported $LiFe_3O_4$ structure described in **Table 2**.

4.4 *In Situ* XRD Analysis during the formation of $LiFe_3O_4$

An important point is that the oxidation state of the $LiFe_3O_4$ phase that is most consistent with XAS, XRD, and neutron characterization is inconsistent with the oxidation state required by the electrochemically discharged amount of lithium. Additionally, the $LiFe_3O_4$ phase it is observed under equilibrium conditions from x=2.0 to 4.0 without evidence for the formation of any other phases despite continued electrochemical reduction. At x=2.0, two electrons have been passed and if all reduction was occurring in the active material, the oxidation state of Fe in the active material should be Fe^{2+}. However, the voltage at which this discharge is occurring coincides with the degradation of the electrolyte observed at potentials below 1.0 V and is likely responsible for the measured discrepancy of Fe redox state.[30]

To better understand the *in situ* formation of the $LiFe_3O_4$ phase and the occurrence of side reactions, *in situ* XRD was taken with the results shown in **Figure 7**. Here, the cell was discharged at a rate of C/25 and during active electrochemistry, the phase change was observed between x = 0 to 3. Observation of the Fe_3O_4(440) and $LiFe_3O_4$(220) reflection intensity indicates the transition begins at approximately x = 0.75 and does not complete until x = 2. After x = 2 there is little to no change in relative peak intensity nor peak position, despite continued electrochemical reduction. This *in situ* diffraction experiment suggests that as much

as one equivalent of lithium is lost in non-Faradaic reaction during discharge between *x*=0-3 and the *ex situ* analysis in **Figure 6** which shows the persistence of the $LiFe_3O_4$ phase from *x*=2-4 indicates that from 3-4 there are no additional structural changes. Combined, these two observations suggest that as much as 2/4 equivalents do not reduce an Fe center from *x*=0-4. This highlights the onset of the formation of the $LiFe_3O_4$ phase during active electrochemistry, and also illustrates that the side reaction occurs during discharge, as nether the peak intensity nor peak positions change with continued discharge from *x*=2-3.

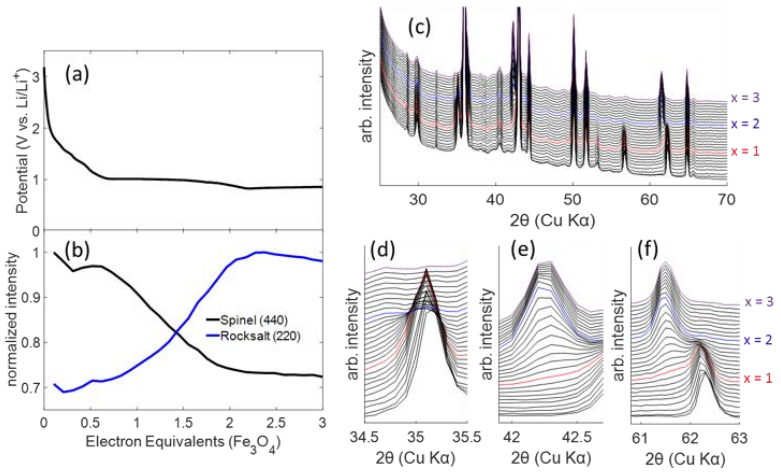

Figure 7: (a) Galvanostatic discharge of the cell with the (b) spinel (440) and rocksalt (220) peak intensities tracked up to *x* = 3 of $Li_xFe_3O_4$. (c) The *in situ* diffraction measurements with the (d) spinel (311) (e) rocksalt (200) and (f) spinel (440) to rocksalt (220) transition highlighted.

5. Conclusions

Systematic refinement iteratively combined with theory were used to describe the lithiation of Fe_3O_4 nanoparticles. Characterization by several methods including XAS, X-ray diffraction and neutron diffraction were utilized. We have discussed nine possible pathways identifies by DFT, and determined the following:

- The XAS analysis, **Figure 3,** indicates no evidence for Fe^0 on the first voltage plateau, despite this prediction on the Li-Fe-O ternary diagram.
- The EXAFS region indicated that the reduction of the Fe in the active material was occurring from *x*=0 to 1.

- The combined XRD and neutron TOF fit, **Figure 5,** allowed for the identification of the $LiFe_3O_4$ phase occurring as the rocksalt phase on the first voltage plateau and eliminated the presence of FeO, Li_2O, and $LiFeO_2$.
- The *in situ* analysis, **Figure 7,** identified that the onset of the $LiFe_3O_4$ rocksalt phase started at x = 0.75 and that this phase did not fully form until x = 2.
- The results of the *ex situ* investigation, **Figure 6,** show the relaxed phase is not the $LiFe_3O_4$ rocksalt phase until x =2. The key reflections that indicate the presence of the $LiFe_3O_4$ phase continue to be observed up until x =4.
- At x =4, the onset of Fe metal formation begins, which indicates that the direct conversion of $LiFe_3O_4$ to Fe metal and Li_2O is possible.

The Li-Fe-O battery system exemplifies the complexity of phase identification in non-ideal systems such as nano-systems and composite electrodes with additives and side reactions. Thorough theoretical studies combined with the systematic refinements with neutron diffraction, X-ray diffraction, and X-ray absorption spectroscopy and electrochemical measurements, the phases occurring on the first phase change plateau were determined to be $LiFe_3O_4$ with the exact structural model reported for the first time. To the authors' knowledge, there has not been another systematic study that has attempted to differentiate the thermodynamic pathway from the kinetic phases observed during discharge in this system, while also eliminating the other possible reaction pathways. The result is that we have definitively identify the equilibrium phase forming on the first voltage plateau as $LiFe_3O_4$. This study illustrates the importance of multidisciplinary experimental, spectroscopic, and theoretical studies for the examination of such processes. This methodologies in this work are broadly applicable to other nano-systems that exhibit phase change behavior as a function of crystallite size and that have suffered from difficult or crystallite-size dependent phase identification.

Supporting Information

Supporting Information is available from the Wiley Online Library.

Conflict of Interest:

These authors report no conflict of interest.

Acknowledgements

C. N. L. and A. M. B. contributed equally to this work. C. N. L. and A. M. B. acknowledge the support of the National Science Foundation Graduate Research Fellowship under Grant Nos. 1644869 and 1109408. Any opinions, findings, and conclusions or recommendations expressed in this material are those of the authors and do not necessarily reflect the views of the National Science Foundation. This work was supported as part of the Center for Mesoscale Transport Properties, an Energy Frontier Research Center supported by the U.S. Department of Energy (DOE), Office of Science, Basic Energy Sciences, under Award DE-SC0012673. A portion of this work was performed using facilities in the Center for Functional Nanomaterials, which is a U.S. DOE Office of Science User Facility, and the Scientific Data and Computing Center, a component of the Computational Science Initiative, at Brookhaven National Laboratory under Contract No. DE-SC0012704. This work also used Columbia University's Shared Research Computing Facility project, which is supported by NIH Research Facility Improvement Grant 1G20RR030893-01, and associated funds from the New York State Empire State Development, Division of Science Technology and Innovation (NYSTAR) Contract C090171, both awarded April 15, 2010. This work also used the Extreme Science and Engineering Discovery Environment (XSEDE), which is supported by National Science Foundation grant number ACI-1548562. XSEDE Stampede and Stampede2 were used through allocation TG-DMR160174 and TG-DMR160128. The neutron diffraction experiments used resources at the Spallation Neutron Source, a DOE Office of Science User Facility operated by the Oak Ridge National Laboratory. Use of the Advanced Photon Source at Argonne National Laboratory for XAS experiments was supported by the U. S. Department of Energy, Office of Science, Office of Basic Energy Sciences, under Contract No. DE-AC02-06CH11357. This x-ray diffraction experiments were conducted at beamline 28-ID of the National Synchrotron Light Source II, a U.S. Department of Energy (DOE) Office of Science User Facility operated for the DOE Office of Science by Brookhaven National Laboratory under Contract No. DE-SC0012704. E.S.T. acknowledges the William and Jane Knapp Chair of Energy and the Environment.

Received: ((will be filled in by the editorial staff))
Revised: ((will be filled in by the editorial staff))
Published online: ((will be filled in by the editorial staff))

References

[1] D. Larcher, C. Masquelier, D. Bonnin, Y. Chabre, V. Masson, J.-B. Leriche, J.-M. Tarascon, *Journal of The Electrochemical Society* 2003, 150, A133.

[2] a) K. He, S. Zhang, J. Li, X. Yu, Q. Meng, Y. Zhu, E. Hu, K. Sun, H. Yun, X.-Q. Yang, Y. Zhu, H. Gan, Y. Mo, E. A. Stach, C. B. Murray, D. Su, *Nature Communications* 2016, 7, 11441; b) D. C. Bock, C. J. Pelliccione, W. Zhang, J. Timoshenko, K. W. Knehr, A. C. West, F. Wang, Y. Li, A. I. Frenkel, E. S. Takeuchi, K. J. Takeuchi, A. C. Marschilok, *Physical Chemistry Chemical Physics* 2017, 19, 20867.

[3] J. Majzlan, A. Navrotsky, U. Schwertmann, *Geochimica et Cosmochimica Acta* 2004, 68, 1049.

[4] M. W. Chase, *J. Phys. Chem. Ref. Data* 1998, Monograph, 1.

[5] H. T. Andersson J.O., Höglund L., Shi P.F., *Calphad* 2002, 26, 273.

[6] H. Liu, H. Liu, S. H. Lapidus, Y. S. Meng, P. J. Chupas, K. W. Chapman, *Journal of The Electrochemical Society* 2017, 164, A1802.

[7] K. W. Knehr, C. A. Cama, N. W. Brady, A. C. Marschilok, K. J. Takeuchi, E. S. Takeuchi, A. C. West, *Electrochimica Acta* 2017, 238, 384.

[8] C. N. Lininger, N. W. Brady, A. C. West, *Accounts of Chemical Research* 2018, 51, 583.

[9] C. C. Yang, Y.-W. Mai, *Materials Science and Engineering: R: Reports* 2014, 79, 1.

[10] a) M. M. Thackeray, L. A. de Picciotto, A. de Kock, P. J. Johnson, V. A. Nicholas, K. T. Adendorff, *Journal of Power Sources* 1987, 21, 1; b) M. M. Thackeray, W. I. F. David, J. B. Goodenough, *Materials Research Bulletin* 1982, 17, 785.

[11] Z. Zhang, S. Satpathy, *Physical Review B* 1991, 44, 13319.

[12] K. E. Sickafus, J. M. Wills, N. W. Grimes, *Journal of the American Ceramic Society* 1999, 82, 3279.

[13] E. Verwey, *Zeitschrift für Kristallographie-Crystalline Materials* 1935, 91, 65.

[14] C. N. Lininger, C. A. Cama, K. J. Takeuchi, A. C. Marschilok, E. S. Takeuchi, A. C. West, M. S. Hybertsen, *Chemistry of Materials* 2018, 30, 7922.

[15] J. Fontcuberta, J. Rodriguez, M. Pernet, G. Longworth, J. B. Goodenough, *J. Appl. Phys.* 1986, 59, 1918.

[16] K. W. Knehr, N. W. Brady, C. N. Lininger, C. A. Cama, D. C. Bock, Z. Lin, A. C. Marschilok, K. J. Takeuchi, E. S. Takeuchi, A. C. West, *ECS Transactions* 2015, 69, 7.

[17] D. C. Bock, G. H. Waller, A. N. Mansour, A. C. Marschilok, K. J. Takeuchi, E. S. Takeuchi, *The Journal of Physical Chemistry C* 2018, 122, 14257.

[18] W. Zhang, D. C. Bock, C. J. Pelliccione, Y. Li, L. Wu, Y. Zhu, A. C. Marschilok, E. S. Takeuchi, K. J. Takeuchi, F. Wang, *Advanced Energy Materials* 2016, 6.

[19] S. Zhu, A. C. Marschilok, E. S. Takeuchi, G. T. Yee, G. Wang, K. J. Takeuchi, *J. Electrochem. Soc.* 2010, 157, A1158.

[20] a) M. Newville, *Journal of Synchrotron Radiation* 2001, 8, 322; b) B. Ravel, M. Newville, *Journal of Synchrotron Radiation* 2005, 12, 537.

[21] J. Mustre de Leon, J. J. Rehr, S. I. Zabinsky, R. C. Albers, *Physical Review B* 1991, 44, 4146.

[22] B. H. Toby, R. B. Von Dreele, *J. Appl. Crystallogr.* 2013, 46, 544.

[23] G. Kresse, J. Furthmüller, *Physical Review B* 1996, 54, 11169.

[24] a) G. Kresse, D. Joubert, *Physical Review B* 1999, 59, 1758; b) P. E. Blöchl, *Physical Review B* 1994, 50, 17953.

[25] a) V. I. Anisimov, J. Zaanen, O. K. Andersen, *Physical Review B* 1991, 44, 943; b) S. L. Dudarev, G. A. Botton, S. Y. Savrasov, Z. Szotek, W. M. Temmerman, A. P. Sutton, *Physica Status Solidi (A)* 1998, 166, 429; c) A. Jain, G. Hautier, S. P. Ong, C. J. Moore, C. C. Fischer, K. A. Persson, G. Ceder, *Physical Review B* 2011, 84, 045115.
[26] J. P. Perdew, K. Burke, Y. Wang, *Physical Review B* 1996, 54, 16533.
[27] a) Y. S. Meng, M. E. Arroyo-de Dompablo, *Energy & Environmental Science* 2009, 2, 589; b) M. S. Islam, C. A. J. Fisher, *Chem. Soc. Rev.* 2014, 43, 185; c) A. Urban, D.-H. Seo, G. Ceder, *Npj Computational Materials* 2016, 2, 16002.
[28] M. C. Menard, A. C. Marschilok, K. J. Takeuchi, E. S. Takeuchi, *Electrochim. Acta* 2013, 94, 320.
[29] N. W. Brady, K. W. Knehr, C. A. Cama, C. N. Lininger, Z. Lin, A. C. Marschilok, K. J. Takeuchi, E. S. Takeuchi, A. C. West, *J. Power Sources* 2016, 321, 106.
[30] M. M. Huie, D. C. Bock, L. Wang, A. C. Marschilok, K. J. Takeuchi, E. S. Takeuchi, *The Journal of Physical Chemistry C* 2018, 122, 10316.
[31] D. Raoux, *Zeitschrift für Physik B Condensed Matter* 1985, 61, 397.
[32] M. Wilke, F. o. Farges, G. E. Brown, Jr., P.-E. Petit, F. o. Martin, *American Mineralogist* 2001, 86, 714.

Keyword Li-ion Batteries

Dr. C. N. L. Author 1, Dr. A. M. B. Author 2, D. M. L. Author 3, L. M. H. Author 4, Prof. K. J. T. Author 5, Prof. E. S. T. Author 6, Dr. A. H. Author 7, Prof. A. C. M. Corresponding Author 8*, Prof. A. C. W. Corresponding Author 9*

Title: The Systematic Refinement for the Phase Change and Conversion Reactions Arising from the Lithiation of Magnetite Nanocrystals

ToC Text: The phases occurring on the open circuit potential for the lithiation of magnetite were identified through iteration between first-principles studies and systematic combined refinement with XAS, XRD, neutron-diffraction, and the measured open circuit potential. This work is broadly applicable to other nano- and meso- scaled systems that exhibit phase change behavior as a function of crystallite size and that have suffered from difficult or crystallite-size dependent phase identification.

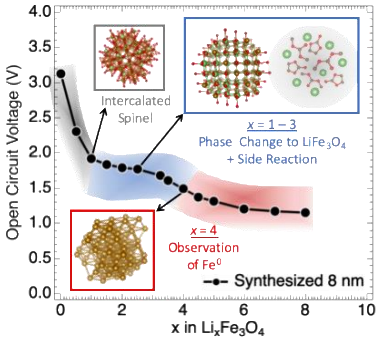

ToC figure

Copyright WILEY-VCH Verlag GmbH & Co. KGaA, 69469 Weinheim, Germany, 2018.

Supporting Information

Title: The Systematic Refinement for the Phase Change and Conversion Reactions Arising from the Lithiation of Magnetite Nanocrystals

Christianna N. Liningerξ, Andrea M. Bruckξ, Diana M. Lutz, Lisa M. Housel , Kenneth J. Takeuchi, Esther S. Takeuchi, Ashfia Huq, Amy C. Marschilok, Alan C. West**

ξThese authors contributed equally to this work.

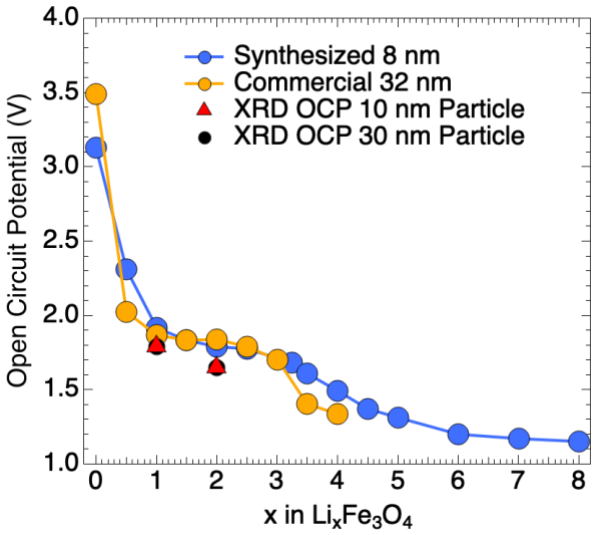

Supporting Figure 1: The open circuit potential for the XRD and neutron diffraction samples that were synthesized following C/600 discharge and voltage relaxation for 10 nm (red triangle) and 30 nm (black circles) compared to previously reported reversible potential curves for 8 nm crystals prepared with co-precipitation and 32 nm commercial crystals discharged at C/200.[1]

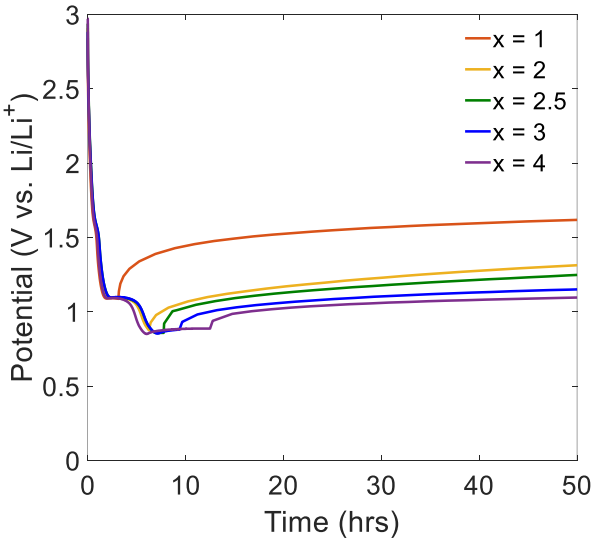

Supporting Figure 2: Galvanostatic discharge and subsequent voltage recovery of the lithiation of $Li_xFe_3O_4$ at x = 1, 2, 2.5, 3, and 4 at a rate of C/25.

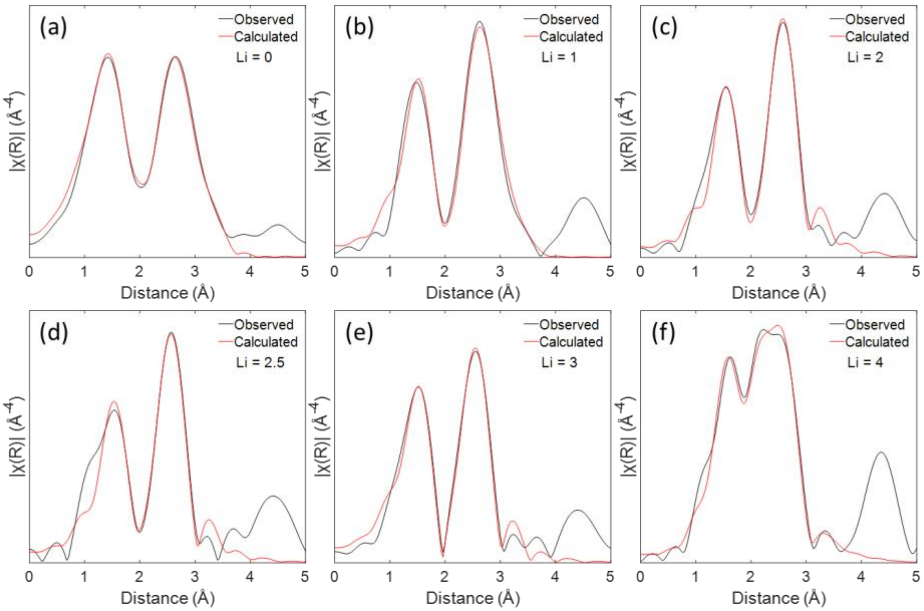

Supporting Figure 3: EXAFS fits at the Fe K-edge of $Li_xFe_3O_4$ lithiated to x = 0, 1, 2, 2.5, 3, and 4 in k-weight = 3 to better identify metal-metal interactions.

Li content	Debye-Waller factor	E_0 (eV)	R factor
0	(Fe) 0.010 +/- 0.002 (O) 0.009 +/- 0.002	- 0.8 +/- 0.8	0.7
1	(Fe) 0.009 +/- 0.002 (O) 0.005 +/- 0.005	- 7 +/- 2	1.6
2	(Fe) 0.012 +/- 0.001 (O) 0.007 +/- 0.002	- 5.5 +/- 0.8	1.9
2.5	(Fe) 0.013 +/- 0.002 (O) 0.009 +/- 0.002	5.8 +/- 0.8	2.3
3	(Fe) 0.012 +/- 0.001 (O) 0.007 +/- 0.001	- 5.7 +/- 0.7	1.6
4	(Fe) 0.010 +/- 0.002 (O) 0.007 +/- 0.004	- 5 +/- 1	1.4

Supporting Table 1: Debye-Waller parameter for Fe and O, E_0, and R factor for EXAFS fits.

Li content	Tetrahedral Iron		Octahedral Iron		Fe Metal
	Fe-O	Fe-Fe	Fe-O	Fe-Fe	Fe-Fe
0	2.15 +/- 0.04 3.75 +/- 0.04	3.47 +/- 0.02 3.62 +/- 0.02	1.96 +/- 0.01 3.56 +/- 0.01	3.01 +/- 0.01 3.52 +/- 0.01	
1	1.90 +/- 0.07 3.50 +/- 0.07	3.40 +/- 0.04 3.56 +/- 0.04	2.04 +/- 0.02 3.65 +/- 0.02	2.99 +/- 0.02 3.51 +/- 0.02	
2			2.07 +/- 0.01 3.66 +/- 0.01	3.045 +/- 0.009	
2.5			2.06 +/- 0.02 3.66 +/- 0.02	3.04 +/- 0.01	
3			2.064 +/- 0.009 3.653 +/- 0.009	3.041 +/- 0.009	
4			2.05 +/- 0.02 3.64 +/- 0.02	3.05 +/- 0.02	2.53 +/- 0.02 2.86 +/- 0.09

Supporting Table 2: Interatomic distances obtained from the EXAFS modeling of x = 0, 1, 2, 2.5, 3, and 4 in $Li_xFe_3O_4$ material.

Li content	Tetrahedral Iron		Octahedral Iron		Fe Metal
	Fe-O	Fe-Fe	Fe-O	Fe-Fe	Fe-Fe
0	1.1 +/- 0.5 3.5 +/- 1.5	3.5 +/- 1.5 1.1 +/- 0.5	3.5 +/- 0.8 3.5 +/- 0.8	3.5 +/- 0.8 3.5 +/- 0.8	
1	1.0 +/- 0.6 2.9 +/- 1.7	2.9 +/- 1.7 1.0 +/- 0.6	2.9 +/- 0.8 2.9 +/- 0.8	2.9 +/- 0.8 2.9 +/- 0.8	
2			4.5 +/- 0.4 3.4 +/- 0.3	6.8 +/- 0.6	
2.5			4.8 +/- 0.6 3.6 +/- 0.4	7.3 +/- 0.8	
3			4.2 +/- 0.4 3.1 +/- 0.3	6.2 +/- 0.8	
4			2.6 +/- 0.6 2.0 +/- 0.4	4 +/- 1	1.1 +/- 0.5 1.5 +/- 0.7

Supporting Table 3: Nearest neighbors obtained from the EXAFS modeling of x = 0, 1, 2, 2.5, 3, and 4 in $Li_xFe_3O_4$ material.

Space group: FeO (Fm-3m), $LiFe_3O_4$ (Fd-3m), Li_2O (Fm-3m),

FeO: a = 4.2317(2) Å
$LiFe_3O_4$: a = 8.4605(3) Å
Li_2O: a = 4.61900 Å

FeO: Phase fraction = 49.3 +/- 0.4%, Crystallite size = 42 +/- 2 nm, Microstrain = 0.09 ± 0.05%, Volume = 75.779(8) $Å^3$
$LiFe_3O_4$: Phase fraction = 45.6%, Crystallite size = 41 nm, Microstrain = 0.24 ± 0.02%, Volume = 605.61(7) $Å^3$
Li_2O: Phase fraction = 5.1%, Crystallite size = 4.0 +/- 0.8 nm, Microstrain = 0.10%, Volume = 98.574 $Å^3$

Atom	x	y	z	Occupancy	Uiso
FeO					
Fe	0	0	0	1.0	0.0237(3)
O	0.5	0.5	0.5	1.0	0.01
$LiFe_3O_4$					
Fe	0.5	0.5	0.5	0.980(1)	0.00300(3)
Fe	0.0	0.0	0.0	0.479(3\1)	0.00300(3)
Li	0.5	0.5	0.5	0.020(1)	0.01
Li	0	0	0	0.521(1)	0.01
O	0.2555(3)	0.2555(3)	0.2555(3)	1.0	0.081
Li_2O					
Li	0.25	0.25	0.25	1.0	0.01
O	0.0	0.0	0.0	1.0	0.01

Neutron: wR = 4.47%, GOF = 3.00
X-ray: wR = 6.94%, GOF = 9.77

Supporting Table 4: Structural parameters for rocksalt structure with the 'FeO + $LiFe_3O_4$+Li_2O' condition obtained from combined Rietveld refinement of TOF neutron diffraction and X-ray diffraction data. Corresponds to DFT Reaction Pathway (h) in Main Text Table 1.

Space group: FeO (Fm-3m), $LiFeO_2$ (R-3m) FeO: a = 4.23150(5) Å $LiFeO_2$: a = 2.9883(6) Å, c = 14.638(2) Å FeO: Phase fraction = 76 +/- 5%, Crystallite size = 43.1 +/- 0.9 nm, Microstrain = 0.15 ± 0.02%, Volume = 75.768(3) $Å^3$ $LiFeO_2$: Phase fraction = 24 +/- 4%, Crystallite size = 38 +/- 2 nm, Microstrain = 0.52 ± 0.09%, Volume = 113.21(3) $Å^3$					
Atom	x	y	z	Occupancy	Uiso
FeO					
Fe	0	0	0	1.0	0.00861(6)
O	0.5	0.5	0.5	1.0	0.01
$LiFeO_2$					
Li	0	0	0	1.0	0.0020(1)
Fe	0	0	0.5	1.0	0.022(2)
O	0	0	0.2470(4)	1.0	0.01
Neutron: wR = 4.75%, GOF = 3.19 X-ray: wR = 7.66%, GOF = 10.79					

Supporting Table 5: Structural parameters for rocksalt structure with the 'FeO + $LiFeO_2$' condition obtained from combined Rietveld refinement of TOF neutron diffraction and X-ray diffraction data. Corresponds to DFT Reaction Pathway (f) in Main Text Table 1.

Space group: FeO (Fm-3m), Li_2O (Fm-3m) FeO: a = 4.23106(6) Å Li_2O: a = 4.61900 Å FeO: Phase fraction = 86.6 +/- 0.7%, Crystallite size = 40 +/- 1 nm, Microstrain = 0.16 ± 0.02%, Volume = 75.744 (3) $Å^3$ Li_2O: Phase fraction = 13 +/- 1%, Crystallite size = 3.9 +/- 0.8 nm, Microstrain = 0.01%, Volume = 98.547 $Å^3$					
Atom	x	y	z	Occupancy	Uiso
FeO					
Fe	0	0	0	1.0	0.00836(7)
O	0.5	0.5	0.5	1.0	0.01
Li_2O					
Li	0.25	0.25	0.25	1.0	0.01
O	0.0	0.0	0.0	1.0	0.01
Neutron: wR = 4.85%, GOF = 3.25 X-ray: wR = 12.95%, GOF = 18.23					

Supporting Table 6: Structural parameters for rocksalt structure with the 'FeO + Li_2O' condition obtained from combined Rietveld refinement of TOF neutron diffraction and X-ray diffraction data. Corresponds to DFT Reaction Pathway (i) in Main Text Table 1.

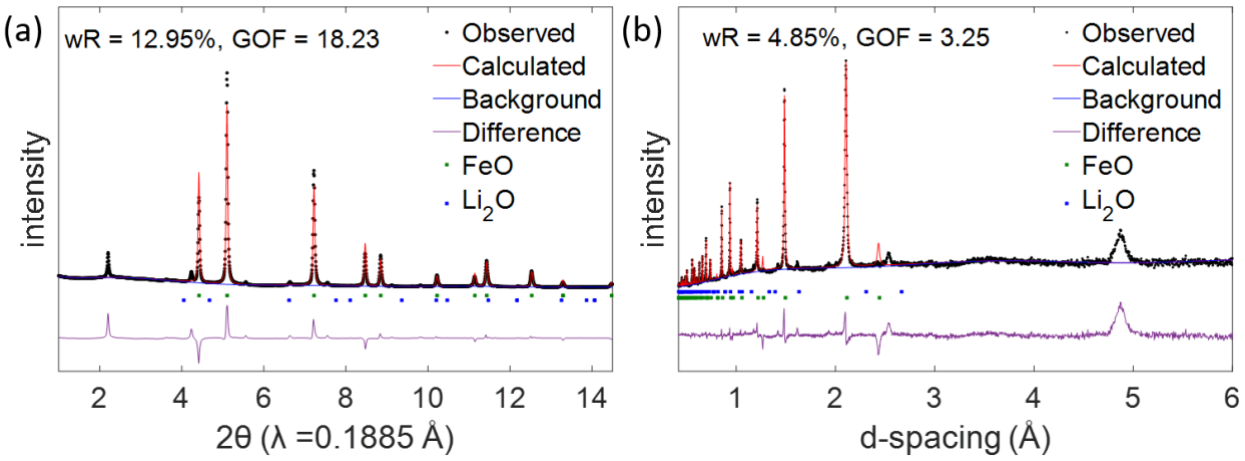

Supporting Figure 4: Rietveld refinement of combined (a) X-ray diffraction and (b) TOF neutron diffraction data for rocksalt structure with the FeO + Li_2O condition. Corresponds to DFT Reaction Pathway (i) in Main Text Table 1.

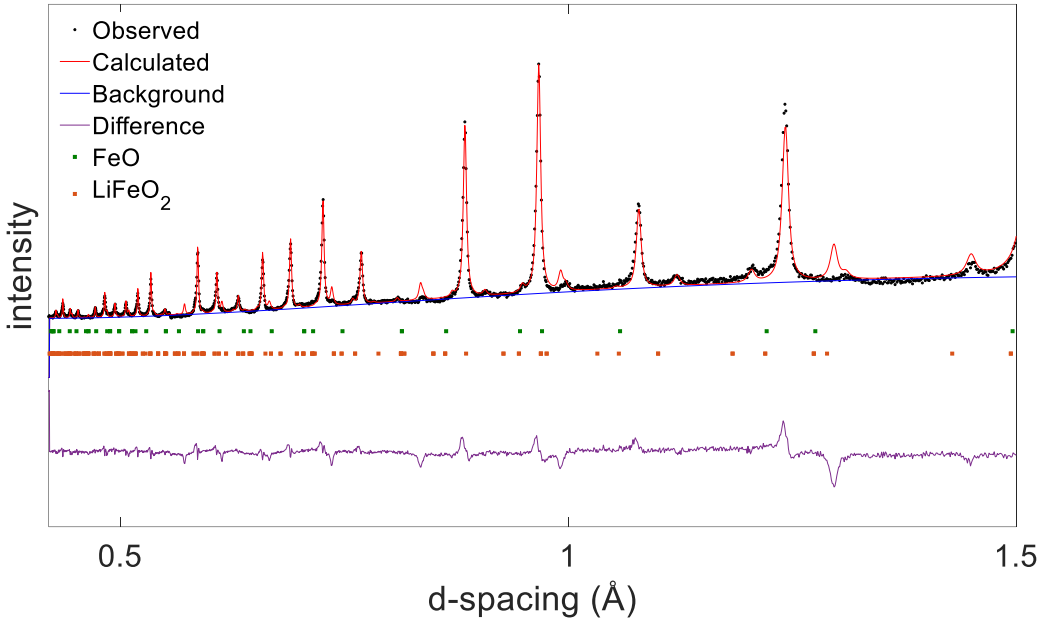

Supporting Figure 5: Rietveld refinement of TOF neutron diffraction below 1.5 Å using the 'FeO + $LiFeO_2$' condition. Corresponds to DFT Reaction Pathway (f) in Main Text Table 1.

Supporting Information References

1. Knehr, K. W.; Cama, C. A.; Brady, N. W.; Marschilok, A. C.; Takeuchi, K. J.; Takeuchi, E. S.; West, A. C., Simulations of Lithium-Magnetite Electrodes Incorporating Phase Change. Electrochimica Acta 2017, 238, 384-396.